Use of Satellite SAR Intensity Imagery for Detecting Building Areas Damaged Due to Earthquakes

Masashi Matsuoka,[a] M.EERI, and Fumio Yamazaki,[b] M.EERI

Synthetic aperture radar (SAR) is remarkable for its capability to record the backscattering coefficient, the physical value of the earth's surface, regardless of weather condition or sun illumination. Therefore, SAR is a powerful tool that can be utilized to develop a universal method to comprehend damaged areas in disasters such as earthquakes, forest fires, and floods. We performed a feasibility study on backscattering characteristics of damaged areas in the 1995 Hyogoken-Nanbu (Kobe), Japan, earthquake using the pre- and post-event ERS images, revealing that the backscattering coefficient and intensity correlation between the two attained values were significantly lowered in hard-hit areas. The evaluation, however, was performed without speckle noise reduction. We also investigated the effects of speckle noise reduction and pixel-window size in evaluating building damage using the difference in the backscattering coefficient and correlation coefficient of the pre- and post-event ERS images. From the analysis, an optimum window size for the damage evaluation was obtained. It was also found that the accuracy of damage detection is not significantly improved for speckle-reduction filtering of window size larger than 21×21 pixels. We developed an automated method to detect hard-hit areas based on the discriminant analysis, and compared the detected distribution with a damage survey result.
[DOI: 10.1193/1.1774182]

INTRODUCTION

From the evaluation of the 1995 Hyogoken-Nanbu (Kobe) and 1994 Northridge earthquakes, we realized the necessity of obtaining disaster information at an early stage. Remote sensing technology and its applications have enabled us to utilize remotely sensed imagery data to assess the vulnerability of urban areas and damage distribution due to natural disasters (Shinozuka and Rejaie 2000, Tralli 2000). Satellite remote sensing, which offers maximal coverage, is useful in providing valuable information to determine damage distribution for recovery activities and restoration planning. A comparison study on satellite optical images with detailed damage survey results reported the spectral characteristics of the damaged areas due to the 1995 Kobe earthquake (Matsuoka and Yamazaki 1998). In the study, we attempted to identify the

[a] Deputy Team Leader, Earthquake Disaster Mitigation Research Center, NIED, 1-5-2 Kaigandori, Wakinohama, Chuo-ku, Kobe 651-0073, Japan
[b] Team Leader, Earthquake Disaster Mitigation Research Center, NIED, 1-5-2 Kaigandori, Wakinohama, Chuo-ku, Kobe 651-0073, Japan

Earthquake Spectra, Volume 20, No. 3, pages 975–994, August 2004;

building damage distribution at a city block level, using the results of field surveys stored in Geographic Information System (GIS) as supervised learning data. Similar approaches comparing pre- and post-disaster satellite optical images were carried out for the 1999 Kocaeli, Turkey, earthquake (Estrada et al. 2000) and the 1990 Luzon, Philippines, earthquake (Yamazaki and Matsuoka 1999).

Among the sensors onboard satellites, synthetic aperture radar (SAR) is one of the most powerful tools for monitoring changes in the earth's surface, and can be used for 24 hours continuously without being influenced by weather condition. SAR systems can image and detect the extent of building damage through clouds and smoke. This feature is quite useful and effective for post-disaster damage assessment, especially when optical remote sensing or a field survey for broad areas is unattainable.

SAR systems are capable of recording both the amplitude and phase of backscattering echoes from the objects on the earth's surface. SAR interferometric analyses using the phase information successfully provided the quantitation of the relative ground displacement level due to natural disasters (Massonnet et al. 1993, Ozawa et al. 1997, Rosen et al. 1999), as well as the inventory of built environment (Eguchi et al. 2000). Using the phase approach, which has a higher level of sensitivity than the intensity approach, correlation between the aggregated damage level of an area and the complex coherence was revealed (Matsuoka and Yamazaki 2000a). The complex coherence obtained from the interferometric analysis, however, is sensitive to satellite geometry, acquisition duration, and wavelengths of radar (Matsuoka and Yamazaki 2000b). The backscattering coefficient of the earth's surface, provided as the amplitude information, is less dependent on the above-mentioned conditions (Yonezawa and Takeuchi 1999). Therefore, the backscattering coefficient derived from SAR intensity images may be used in developing a universal method to capture damaged areas just after natural disasters.

Since the spatial resolution of operated satellites is fairly coarse, i.e., roughly 30 meters, it is difficult to identify the backscattering characteristics of individual buildings. However, it is possible to detect the groups of damaged buildings. Therefore, in order to extract the extent of building damage in an area, we should consider aggregated information such as average, texture, and correlation within a local window. In this study, we introduce the characteristic changes in the backscattering coefficient for extensively damaged areas using a GIS data set for the Kobe earthquake. The effects of pixel-window size and SAR speckle noise are examined in evaluating building damage, using the difference in the backscattering coefficient and spatial correlation between the pre- and post-event images. Finally, we propose an automated method to detect hard-hit areas using SAR intensity images after speckle noise reduction.

BASIC PRINCIPLES OF SAR

SAR, which is one of the active remote sensing techniques, transmits a microwave signal toward a target and receives its reflection (amplitude and phase) back to the sensor or antenna (Henderson and Lewis 1998). Normally, the wavelength is in the order of 1 cm to 1 m, corresponding to a frequency range of about 30 GHz to 300 MHz. A SAR system can be boarded on both airborne and spaceborne platforms. SAR creates rela-

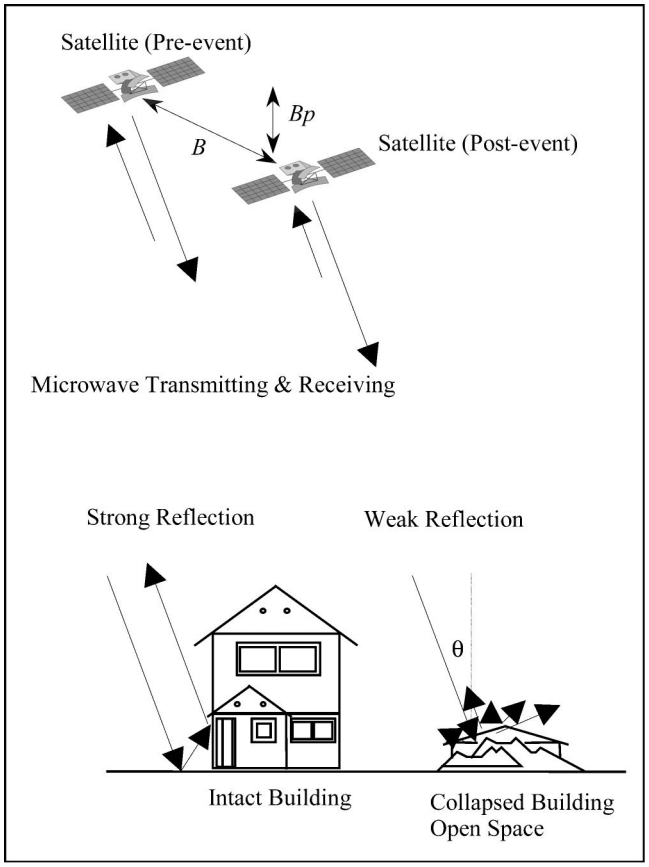

Figure 1. Schematic figure of the geometry of repeat-pass satellite observation and backscattering characteristics of objects on the earth's surface.

tively high ground (pixel) resolution because it simulates a long antenna by combining electrical signals received by its sensor as it moves along a particular flight track. Each pixel in an amplitude (intensity) image represents the radar backscattering strength for that area on the ground. "The backscattering coefficient" is dependent on the roughness of the surface, the moisture level of the area, and the incident angle of a microwave and its wavelength. According to our previous studies for evaluating the backscatter in the 1995 Kobe earthquake (Aoki et al. 1998, Matsuoka and Yamazaki 2000b), man-made structures show comparatively high reflection due to multiple reflections, called the "cardinal effect" or "corner reflector" between structures and ground. Open spaces or damaged buildings have comparatively low reflectance because microwaves are scattered in different directions. A schematic diagram of surface objects and their backscattering properties are shown in Figure 1. Buildings may be reduced to debris by an earthquake, and in some cases, the debris of buildings may be removed, leaving the ground exposed. Thus the backscattering coefficient determined after damage is likely to be lowered,

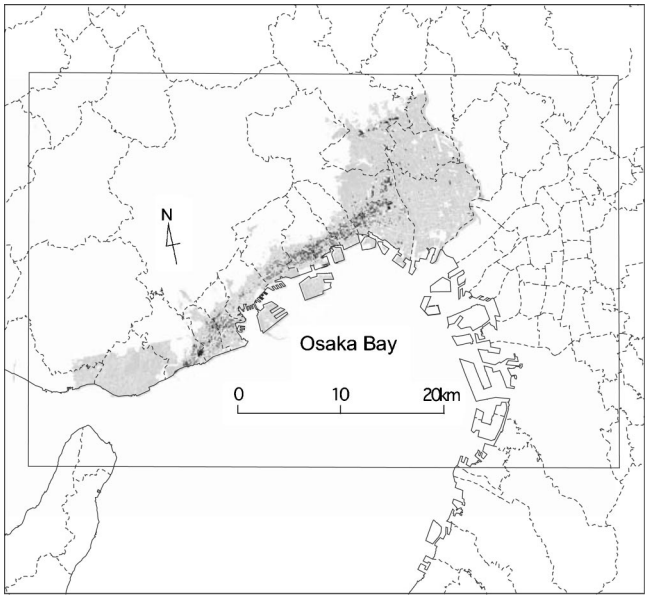

Figure 2. The area of this study. The area inside the rectangle indicates the ERS/SAR image. The shaded area indicates the coverage of the building damage survey data (BRI 1996) and the dark spots show the city blocks with a severe damage ratio of more than 30% in the damage survey.

compared to that obtained before the event. For comparing two acquisition data, an image-matching process with high accuracy is needed. In the case of using airborne sensors, a slight difference in two airplane orbits causes great difficulty in pixel-by-pixel matching, because of their high spatial resolution. However, the image-matching of satellite SAR images does not create a significant problem when we use the images taken by a same satellite system.

In the next section, we quantitatively evaluate the backscattering characteristics of the areas with building damage due to the Kobe earthquake, as detailed damage survey results of this event are stored in GIS.

DATA SET

SAR DATA AND IMAGE PROCESSING

Several satellites observed the Kobe area before and after the Kobe earthquake (Sudo et al. 1995), which occurred on 17 January 1995. We used European Remote Sensing (ERS) satellite images acquired on 23 May 1995, 1 August 1995, 27 February 1996, 2 April 1996, and 10 September 1997 as post-event data and those taken on 12 October 1994, 3 June 1994, 8 August 1993, and 1 November 1992 as pre-event data, respectively. The coverage of the satellite images is shown in Figure 2. Based on this time-series data set, we examined and monitored the change in backscattering characteristics of damaged

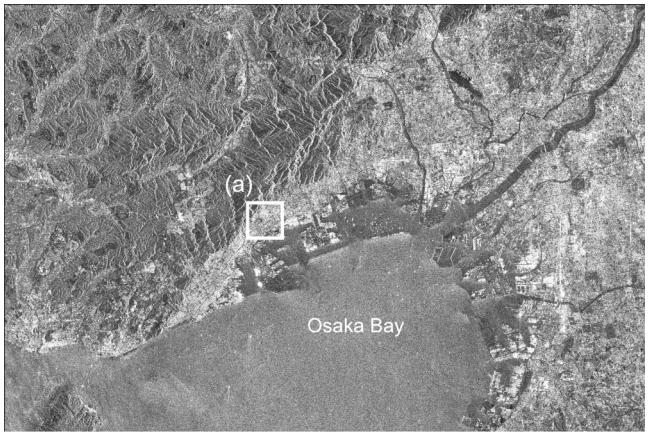

Figure 3. Backscattered intensity image of ERS/SAR taken after the 1995 Kobe earthquake (23 May, 1995).

and nondamaged areas. The image shown in Figure 3 was obtained on the closest date after the earthquake (i.e., four months after the event). From December 1993 to March 1995, the orbit of the ERS satellite was changed and periodic observation was made impossible; the first image observing the damaged area was taken four months after the earthquake (Massonnet et al. 1996). When the ERS satellite obtained the last pre-event image, therefore, it was in the course of orbit alteration, i.e., the orbit was completely different from that of post-earthquake.

From our visual inspection using aerial photographs taken in May 1995, some of the severely damaged buildings had already been demolished and open spaces were exposed in this period. Due to the elapsed period, a direct comparison between the SAR images and the field survey data may be inaccurate, but we assume that basic evaluation is still possible on the potentiality of satellite SAR images in detecting the changes in the earth's surface of urban areas.

The major characteristics of ERS/SAR systems are listed in Table 1. One pixel is equivalent to a ground distance of 30 m, and its digital number was converted into a

Table 1. Characteristics of European Remote Sensing (ERS) satellite

Frequency	5.3GHz (C-band)
Wavelength	5.7 cm
Polarization	VV
Incidence Angle	23°
Swath Width	100 km
Spatial Resolution	30 m
Recurrence Period	35 days

power of the radar brightness. All the intensity images were matched to the 23 May 1995 data by the nearest-neighborhood method, using several tie points obtained from the optimal pixel pair selection, by searching pixel by pixel, at the position that yields the highest correlation for the area of the 7×7-pixel window between the two intensity images, i.e., template matching technique. Correlation and difference in the backscattering coefficient of the two acquisitions were used as the indices representing the changes in affected areas. The correlation coefficient, r, between two intensity images, a and b, was calculated within a small corresponding window as follows:

$$r=\frac{N\Sigma_{i=1}^{N}Ia_iIb_i-\Sigma_{i=1}^{N}Ia_i\Sigma_{i=1}^{N}Ib_i}{\sqrt{(N\Sigma_{i=1}^{N}Ia_i^2-(\Sigma_{i=1}^{N}Ia_i)^2)\cdot(N\Sigma_{i=1}^{N}Ib_i^2-(\Sigma_{i=1}^{N}Ib_i)^2)}} \tag{1}$$

where i is the sample number, Ia_i and Ib_i are the digital numbers of the two images, and N is the total number of pixels within a small window. We created correlation images for the calculation pixel size, which is changed from a 3×3- to a 51×51-pixel window. The range of the correlation coefficient, r, is between −1.0 and 1.0. If there is any big spatial difference between the images of two acquisitions within a local window, the correlation coefficient of the center pixel gains a small value. Adversely, if an area has completely no change within a local window, the correlation coefficient should be 1.0. The difference in backscattering coefficient, d, for the pair was calculated by averaging within a small corresponding window, in a manner similar to that of the correlation calculation, which is shown in Equation 2:

$$d=10\cdot\log_{10}\overline{Ia}_i-10\cdot\log_{10}\overline{Ib}_i \tag{2}$$

where i is the sample number, and $\overline{Ia}_i$ and $\overline{Ib}_i$ are the corresponding averaged digital numbers over the surroundings of pixel i within a small window. Then the images of the intensity difference were generated. All the executed images were registered using the affine geometric correction to overlay with damage survey data as described in a later section.

It should be pointed out that under a condition where the phase information can be used, spatial grasping of relative crustal movement (Massonnet et al. 1993, Ozawa et al. 1997) is possible by means of interferometric processing. The areas containing few damaged buildings can also be detected from the indices (coherence) that represent the degree of correlation of the phase information (Matsuoka and Yamazaki 2000a, Ito et al. 2000, Yonezawa and Takeuchi 2001). The condition in this case is the distance of two satellites and the time interval of two observations. When the perpendicular separation of the two satellites (the baseline), B_p, shown in Figure 1 is long, coherence of an image as a whole is reduced, and low coherence areas (damaged areas) become difficult to find out. When the observation interval is very long, not only the target variance but also the secular change are detected, and it becomes difficult to distinguish the two.

For the latter problem, a model that estimates damage level was proposed evaluating the reduction of coherence with time, introducing a coherence ratio (Ito et al. 2000). In this model, however, the reduction of the coherence S/N ratio caused by the distance of two satellites is unavoidable. The primary condition to identify damaged and nondam-

aged areas from the coherence, therefore, is that the satellites orbits of two acquisition dates are close (Matsuoka and Yamazaki 2000b, Yonezawa and Takeuchi 2001). Satisfing these conditions, in case of the 1995 Hyogoken-Nanbu earthquake, we are lucky that JERS (Japanese Earth Resources Satellite) observed the affected area twenty days after the earthquake (Ozawa et al. 1997), while ERS images were taken almost one year after the earthquake, due to the timing of satellites orbit change.

For the 1994 Northridge earthquake, images suitable for interferometric study were obtained by JERS a half year later (Massonnet et al. 1996, Murakami et al. 1996), and by ERS one year and three months after the earthquake (Massonnet et al. 1996). At the moment, observation opportunities whose coherences are available are rather limited. It is, however, pointed out that satellites to be launched in the future are capable of highly accurate orbit control, and images suitable for interference will increase significantly. On the other hand, as to the intensity correlation, variation of texture patterns is equivalent to coherence (Zebker and Villasenor 1992); it is shown that the influence of the distance between two satellites is rather small in case of intensity correlation in urbanized areas from the observation fact (Yonezawa and Takeuchi 2001). We think it an essential prerequisite to use indices that are independent of observation conditions, in order to put remote sensing technology to practical use in damage grasping at the time of natural disasters or emergency; hence we only use intensity information in this study.

DAMAGE SURVEY DATA

In this study, we focus on building damage as one of the primary forms of earthquake impact. The GIS building damage data was provided based on detailed survey results compiled by AIJ (the Architectural Institute of Japan) and CPIJ (the City Planning Institute of Japan), and digitized by BRI (Building Research Institute), wherein the building damage level is classified into five categories: damage by fire, severe damage, moderate damage, slight damage, and no damage, with the number of damaged buildings being totaled for each city-block in each ward (BRI 1996). Severe damage almost corresponds to D5～D4 and a part of D3 in the classification of the European Macroseismic Scale (EMS) (Maki et al. 2001). The affected areas (where building damage occurred at least to some extent) and the severely damaged zone were calculated from the GIS data (Figure 2). The histogram for the area of each city block in Kobe and Osaka is shown in Figure 4. The average size of city blocks is approximately 5,000 square meters.

PRELIMINARY ANALYSIS OF BACKSCATTERING CHARACTERISTICS IN THE AREAS WITH BUILDING DAMAGE USING ORIGINAL SAR IMAGES

Using the field survey data, the damage ratio of buildings at a city-block level was calculated as the ratio between the number of buildings classified as burnt or severely damaged and the total number of buildings in each block. The damage level was classified into seven categories, A, B, C, D, E, F, and G, corresponding to no damage, damage ratios of 0–6.25, 6.25–12.5, 12.5–25, 25–50, 50–100%, and 100%, respectively, based on the severity of damage. The pixels that correspond to the area of each damage class were selected in order to examine the difference in the backscattering coefficient and correlation coefficient in the damaged areas. The class with no damage (A) includes the

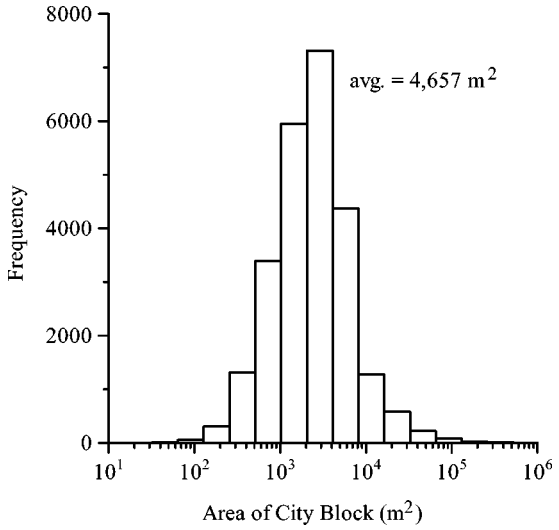

Figure 4. Histogram for the areas of city blocks in cities of Kobe and Osaka.

pixels of buildings with no exterior evidence of damage according to the field survey. The 2,000 pixels for each damage class were selected for the analysis. The backscattering coefficients of most of the selected pixels were high, approximately more than −5 dB, because of the cardinal effect in urban areas. There was slight variation in the SAR images due to vegetation, which we disregarded in this study.

By assigning the images taken on 12 October 1994 and 23 May 1995 as the master (image *b*) and slave (image *a*), respectively, utilizing the 5×5-pixel window for calculating the two indices, we previously reported that the difference of the backscattering coefficient (after–before) becomes higher and negative while the correlation coefficient becomes lower in the area showing high damage ratios (Aoki et al. 1998). One of the major reasons of this observation is that collapsed buildings and debris create the loss of corner reflectors. On the other hand, in the area with low damage ratios, the difference of the backscattering coefficients becomes lower and the correlation coefficient becomes higher. We tried to extract damage areas by a simple classification technique. The areas corresponding to severe damage or complete damage (G) and the area with no damage (A) were selected because these areas exhibit the highest deviation in their differences of the backscattering coefficient and correlation coefficient. A linear discriminant analysis was used to classify these areas (Figure 5). Since the standard deviations of these two indices for each damage class are significantly high, the coincidence ratio obtained from the analysis is not of an acceptable level for a practical use. The vast randomness was likely to be caused by the following reasons:

1. The observation conditions, such as the satellite orbit, atmosphere, and surface moisture at the two acquisition times were not equal;

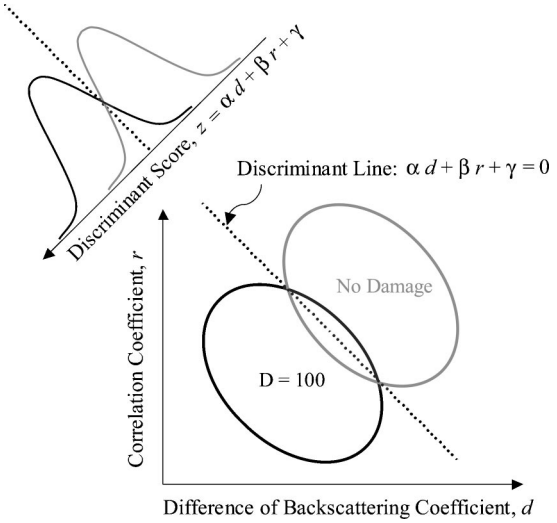

Figure 5. Schematic figure of discrimination between the area where the severe damage ratio (D) equals to 100% and that with no damage using two indices, the difference of backscattering coefficient and the spatial correlation coefficient.

2. Even in the area with no damage, the difference in the earth's surface, whether it is covered by buildings or vegetation, and temporal changes of two acquisition data existed;
3. Even in the severely damaged area where the damage ratio equaled to 100%, the training data possibly include not only collapsed or severely damaged buildings but also open spaces within the city block (Figure 6); and
4. Quality of the intensity images could be degraded by an ineluctable potential noise called "the speckle noise" from a SAR system (Ulaby et al. 1982).

Among the possible reasons listed above, the effects of the speckle noise could have been decreased by image processing. In general, the speckle noise can be reduced by averaging pixel values for an area in a window in a manner similar to the pseudo multilook processing, as well as by applying speckle reduction filters for the SAR intensity image.

EFFECTS OF SPECKLE NOISE ON DAMAGE DISTRIBUTION DETECTION

WINDOW SIZE FOR COMPUTING BACKSCATTERING INDICES

Our previous study used the window size of 5×5 pixels (approximately 150×150 square meters) in calculating the average difference and the spatial correlation (Aoki et al. 1998). However, we are uncertain whether this model is optimal or appropriate for damage evaluation. Yonezawa and Takeuchi (2001) suggested that the accuracy of interpreting damaged and intact areas increases when the window for computing the spatial correlation is enlarged. In this section, we examine the relationship between the accu-

Figure 6. Size of pixels in ERS image compared to actual buildings and city blocks. Thick black grid indicates the pixels representing the areas with the severe damage ratio equals to 100%.

racy in damage detection and the window size for computing the two indices. We changed the window size from 3×3 to 51×51 pixels and calculated the indices in the window, and then calculated the coincidence ratio of discrimination for the areas where the damage ratio equals 100%, as well as for the areas with no damage. The relationship for the calculation window size, its dimension (area), and the coincidence ratio are shown in Figure 7. It is observed that as the window size becomes larger, the accuracy of discrimination becomes higher. A 21×21-pixel window exhibited the highest coincidence ratio.

A relatively large window size is needed to capture the severely damaged buildings in spatial distribution. Also, the speckle noise may be reduced slightly by using the average value inside a calculation window. If the window size is chosen to be over 31 ×31 pixels, the coincidence ratio may decrease due to the existence of severely damaged buildings even in the areas selected for the class with no damage, and the reverse situation is also plausible.

The above-mentioned optimal window size for maximizing the ability to distinguish severely damaged and nondamaged areas was derived only from the data set for the 1995 Kobe earthquake. This optimal value may change if the condition of urban areas and the spatial resolution of satellite images are different from those of the Kobe case.

EFFECT OF SPECKLE REDUCTION FILTERING

We examined the effect of speckle reduction filters on the accuracy of damage detection in SAR intensity images. Three typical filters, median, Lee (Lee 1980), and Frost (Frost et al. 1982), were applied to the pre- and post-event registered images. A spatial

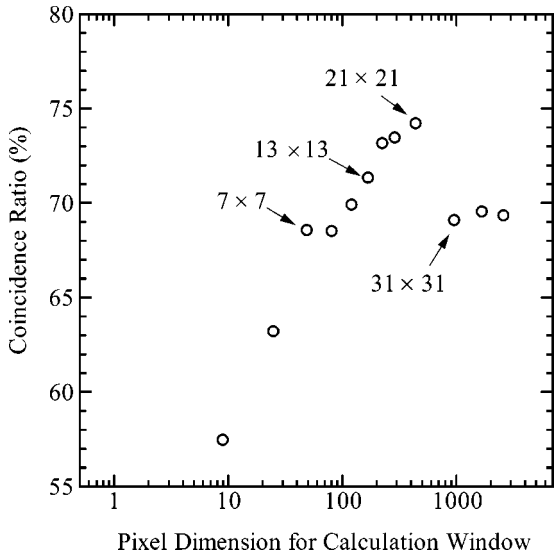

Figure 7. Relationship between accuracy for detecting building damage and dimension of window for computing two indices.

filtering is a local operation for the pixel values in an original SAR intensity image. During the filtering, the pixel values were modified using the values of neighboring pixels. The zoom-up image of a rectangle area (Figure 3a) applied by each filter is shown in Figure 8. The window size for filtering was 5×5 pixels. To exhibit the filtered images, we conducted an enhancement process to improve the visual interpretability of the images using the histogram stretch method. In comparison with the original image shown in Figure 8a, low-frequency features are enhanced in the median-filtered image (Figure 8b), and a block boundary, such as roads, is clearly observed in the images filtered by Lee and Frost (Figures 8c and d).

After computing the difference in the backscattering coefficient and correlation coefficient within the areas of 7×7, 13×13, and 21×21 pixels using the pre- and post-event filtered images, the discriminant analysis for areas with no damage and those sustained severe damage was carried out. Figure 9 shows the coincidence ratios by the discriminant functions for each of the filtered and original images. Although the 7-by-7-pixel window applied to the Median-filtered image exhibits a low coincidence ratio, all the other filtered images show higher ratios than that of the original image, demonstrating that the speckle reduction filters improve the accuracy of building damage detection. The accuracy of damage detection using the Lee- or Frost-filtered SAR intensity images is relatively high among the three filter types.

Next, the relationship between the speckle reduction filter size and the accuracy of damage detection was investigated. We used the Lee filter because of its simple design and rather higher coincidence ratio shown during the damage evaluation. We changed the filtering window size from 3×3 to 51×51 pixels and measured the changes in the

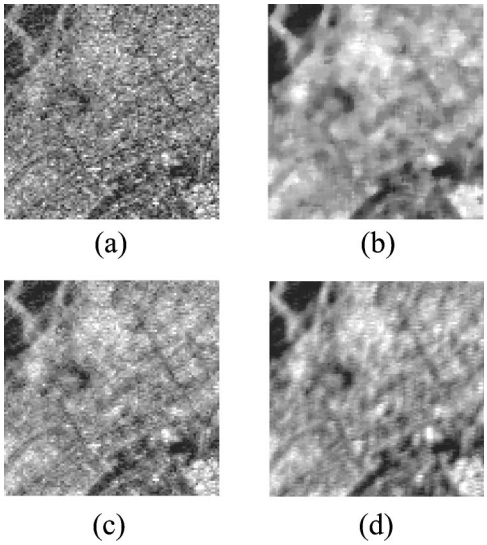

Figure 8. Original image and images filtered for speckle reduction by typical 5×5-pixel windows: (a) original, (b) median filter, (c) Lee filter, and (d) Frost filter.

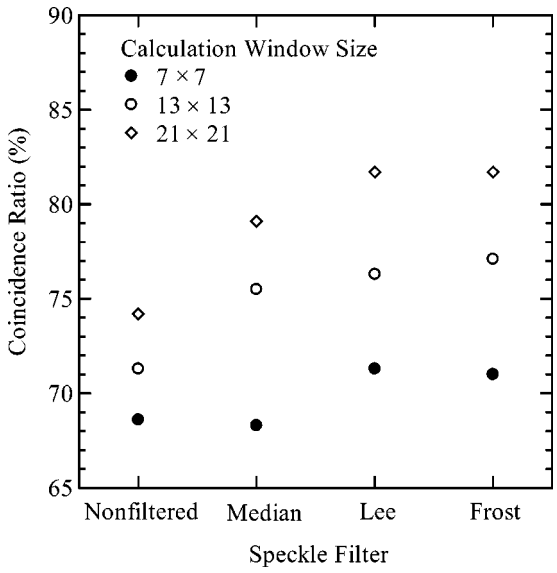

Figure 9. Accuracy for detecting building damage for original image and each image filtered by 5×5-pixel window. Solid circle, hollow circle, and hollow diamond indicate the dimension of the window to compute two indices for 7×7 pixels, 13×13 pixels, and 21×21 pixels, respectively.

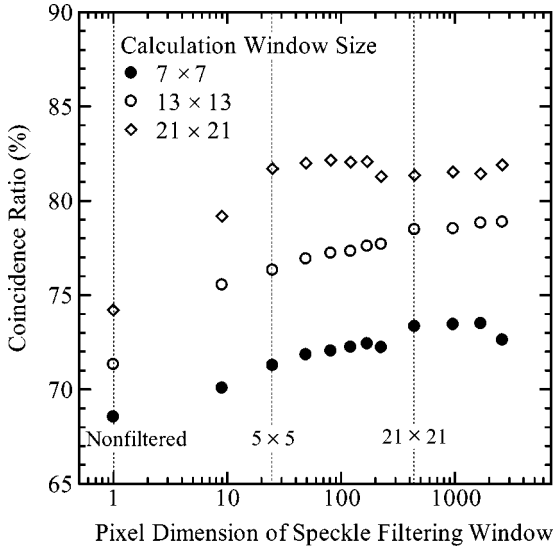

Figure 10. Relationship between the accuracy for detecting building damage and dimension of window for Lee filtering. Solid circle, hollow circle, and hollow diamond indicate the sizes of window to compute two indices for 7×7 pixels, 13×13 pixels, and 21×21 pixels, respectively.

coincidence ratio (Figure 10). Regardless of the window size used for computing the two indices (the average difference and correlation coefficient), as the filter size became larger, the coincidence ratio became higher. A similar trend in the coincidence ratio was observed for the calculation window size of 7×7 and 13×13 pixels, and the coincidence ratio was almost saturated at the 21×21-pixel window for filtering. In contrast, for the 21×21-pixel window used for computing the two indices, the coincidence ratio is seen to be saturated at the 5×5-pixel window for filtering. In the previous section, 21×21 pixels, which exhibited the highest coincidence ratio, is considered to be the optimal window size for damage evaluation. It has also been discovered that the accuracy of damage detection is not significantly increased in speckle-reduction filtering of window size larger than 21×21 pixels. It is noteworthy that the 21×21 pixels is a criterion for both window sizes.

IDENTIFICATION OF BUILDING DAMAGE AREAS

IDENTIFICATION OF TEMPORAL CHARACTERISTICS OF BACKSCATTERING INDICES IN BUILDING DAMAGE AREAS

When the window size of 21×21 pixels was used in the above-mentioned analysis, higher discriminant accuracy between the damaged and nondamaged areas was obtained. Image processing using a large window size may result in rough estimation and can only be utilized for widespread severe damage. A larger window size, however, does not offer the capability for detecting small spatial changes within a window. As shown in Figure 10, the difference in coincidence ratios using the window size of 13×13 pixels and 21

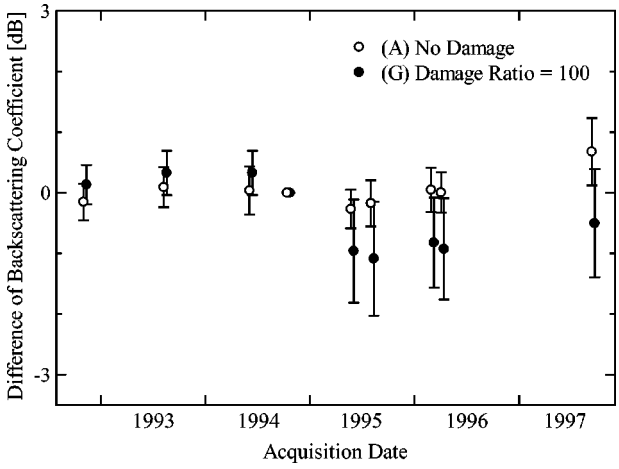

Figure 11. Temporal characteristics of the difference in backscattering coefficient with respect to the image taken on 12 October 1994. Hollow and solid circles indicate mean values; error bars indicate standard deviation for nondamaged and severely damaged areas, respectively.

×21 pixels is not so distinct, particularly when images employ the Lee filter larger than 21×21 pixels. Therefore, we decided to use a 13×13-pixel window in this study to compute the two indices from two acquisition data in order to detect small features. Based on the results of the above analyses, a temporal change in the two indices through a time-series analysis was investigated. We assigned the image taken on 12 October 1994 as a master (image *b*), and the other as slave (image *a*). Then the two indices were calculated by Equations 1 and 2 using two acquisition images, *a* and *b*.

Figure 11 shows the temporal characteristics of the difference in the areas where the severely damaged ratio equals 100% and those with no damage. The mean values of the difference in the backscattering coefficient in the damaged areas see a decrease to approximately −1 dB after the event. So far, the standard deviation in the damaged areas looks relatively large after the earthquake. On the other hand, we could not readily observe any trends in the mean value for the areas without damage during the period of the earthquake occurrence. Furthermore, in the damaged areas, the trend is seen for the value that decreased immediately after the event and then increased gradually until the year 1997. The influence of the observation conditions, such as the satellite orbit, was possibly included in this trend besides the change of the scattering condition in the earth's surface, as the value increased similarly in the areas without damage as well. The temporal change in the correlation coefficient for the both areas is shown in Figure 12. The mean values of the correlation coefficient for both the severely damaged and nondamaged areas were nearly the same, around 0.6 before the earthquake, however, the value for the severely damaged area after the earthquake decreased to approximately 0.3, and then remained at constant level. The scatter in the mean value of the correlation coefficient is seen to be more stable than that of the mean value of the difference in the backscattering coefficient (see Figure 11).

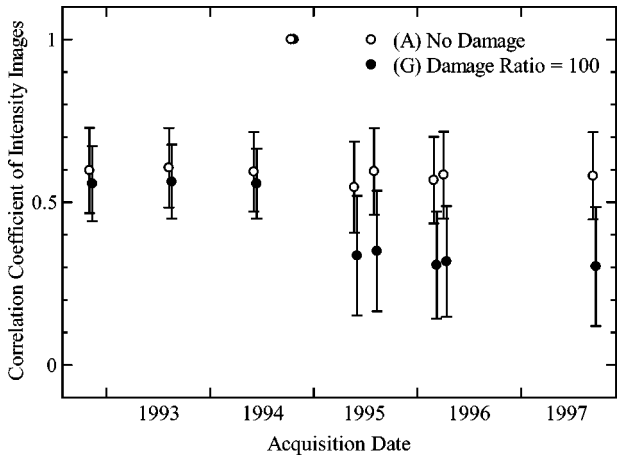

Figure 12. Temporal characteristics of the spatial correlation coefficient with respect to the image taken on 12 October 1994. Hollow and solid circles indicate mean values; error bars indicate standard deviation for nondamaged and severely damaged areas, respectively.

DETECTION OF BUILDING DAMAGE DISTRIBUTION

This study demonstrates that the severely damaged areas can be identified with two simple indices when using the time-series SAR data. The difference between the backscattering coefficient, d, and the correlation coefficient, r, for each area was obtained from the corresponding 13×13-pixel window using a pair of images, from 23 May 1995 and 12 October 1994, which have been filtered by Lee of a 21×21-pixel window (Figure 13). A linear discriminant analysis shown in Figure 5 was applied to classify severely damaged and nondamaged areas. A discriminant formula, shown in dotted lines in Figure 13 obtained from the analysis, is indicated in Equation 3:

$$z = -2.140\ d - 12.465\ r + 4.183 \tag{3}$$

where z is the discriminant score. According to the probability in this discriminant analysis for the two conditions, the pixels whose value z is positive and negative are assigned as severe damage and no damage, respectively. Because the both coefficients are negative, the higher and negative d or the smaller r gains the lager z. The coincidence ratio of the discrimination for the two conditions was 78.5% based on this training data set. When we considered the only single measure, i.e., difference or correlation, the results of the coincidence ratio for distinguish the two conditions by uni-variate Mahalanobis' generalized distance using the difference or the correlation were 71.1% and 73.4%, respectively. The accuracy of the discrimination with the both measures together shows higher than that using one of the measures.

In applying this Equation 3 to the seven categories of the whole training data set, the mean and standard deviation for severe damage ratios were computed as shown in Table 2. The discriminant score z indicates the degree of building damage in the area. The distribution of value z overlaid on the SAR original intensity image is depicted in Figure

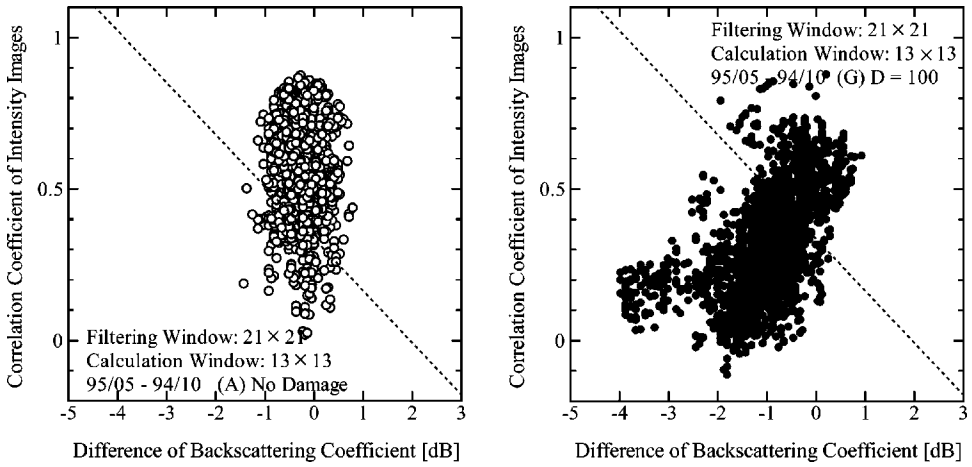

Figure 13. Difference in the backscattering coefficient and correlation coefficient between the areas with (a) no damage and where (b) the severe damage ratio equals to 100%.

14. The darker area shows the pixels with higher z value. Focusing on urbanized areas to detect building damage, the pixels whose backscattering coefficients are smaller than the assigned threshold value (-5 dB) were masked in the plot due to the backscattering reflection generally being stronger in highly developed areas than other areas, such as the sea and areas with a large amount of vegetation. In this figure, the dark area constitutes a belt that is similar to the hard-hit zone based on the field survey, shown in Figure 2. It is conceivable that the backscattered intensity decreased in the damaged area due to the reduction of the cardinal effect of microwaves since buildings were collapsed and/or removed and vacant spaces were formed. The flow and notes for the image processing to detect the damaged area is summarized in Figure 15.

Although comprehending overall damage distribution is possible from existing satellites, high-resolution spaceborne or airborne SAR remote sensing, which collects further detailed damage information on built environment, will be realized in the near fu-

Table 2. Mean and standard deviation of discriminant score (z) for the classified damaged area

Damage level Severe damage ratio: D (%)	Number of pixels	Discriminant score: z Mean (Standard deviation)
(A) No Damage	**2000**	**−2.053(1.862)**
(B) $D<6.25$	2000	−1.918(2.018)
(C) $D<12.5$	2000	−1.244(2.230)
(D) $D<25$	2000	−0.602(2.436)
(E) $D<50$	2000	0.320(2.851)
(F) $D<100$	2000	1.803(3.263)
(G) D=100	**2000**	**2.053(3.595)**

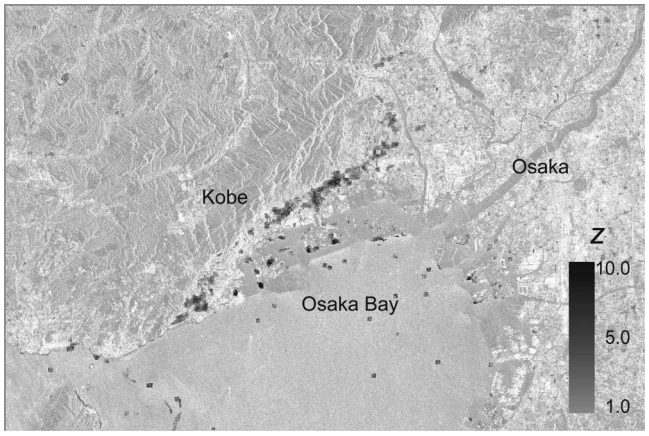

Figure 14. Distribution of the value z overlaid on the intensity image taken on 12 October 1994.

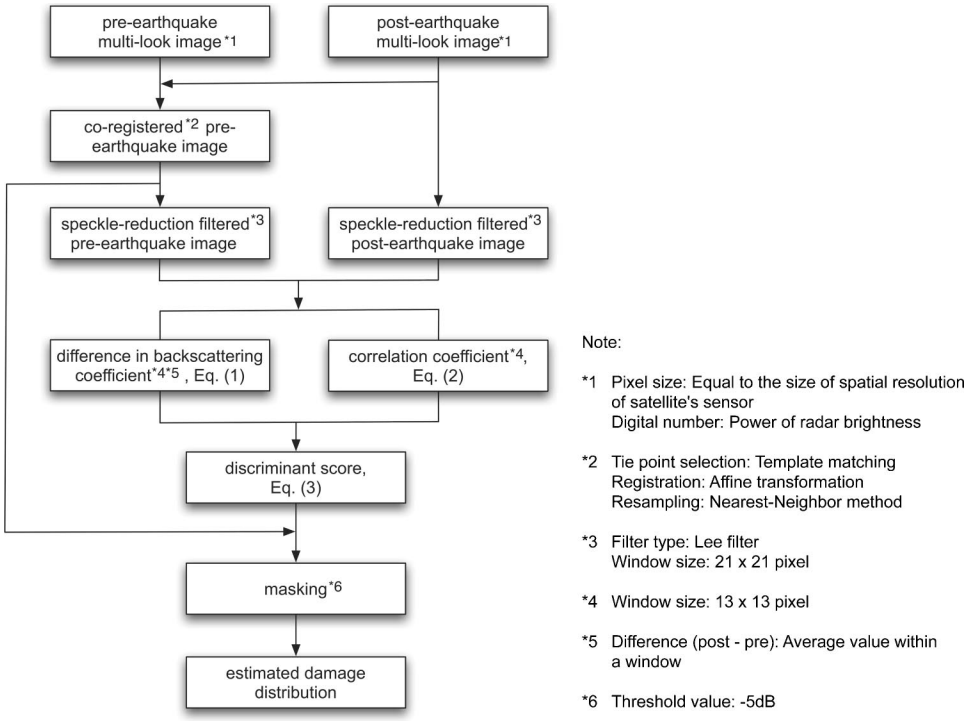

Figure 15. Flowchart and notes for image processing to detect areas with building damage.

ture. A theoretical study on evaluating the deformation of actual-size buildings by simulated SAR imagery based on an electromagnetic formulation (Shinozuka et al. 2000) will prove to be informative in ascertaining this objective.

CONCLUSIONS

Quantitative evaluation on the characteristics of satellite SAR images of the damaged area was conducted using ERS/SAR data obtained before and after the 1995 Hyogoken-Nanbu (Kobe) earthquake. In our previous study, the correlation between the building damage ratio and satellite SAR image indicated a trend regarding the building damage ratio; in the area with a high damage ratio, the difference of the backscattering coefficient (after–before) becomes higher and negative, and the correlation coefficient becomes lower. To develop a universal method for identifying damaged areas, a parametric study was conducted for selecting the optimal window size for computing the two indices and the difference and correlation to distinguish severely damaged and nondamaged areas. The effects of the speckle noise reduction filter for evaluating the building damage were also examined. From this analysis, the application of the discriminant score, which is derived from the combination of two indices within a corresponding window using the pre- and post-event speckle-reduction filtered images, was proposed to detect severely damaged areas. The distribution obtained from this procedure showed relatively good agreement with the actual damage distribution by the field survey. Since this damage detection method was developed based on the data set only from the Kobe earthquake, a further study is needed through information from other recent destructive earthquakes in the world to be able to reach a general consensus for earthquake damage detection in urban areas using satellite SAR.

ACKNOWLEDGMENTS

We would like to thank Dr. Nobuoto Nojima of Gifu University for his helpful advice on the discriminant analysis. The ERS/SAR images used in this study are owned by the European Space Agency (ESA).

REFERENCES

Aoki, H., Matsuoka, M., and Yamazaki, F., 1998. Characteristics of satellite SAR images in the damaged areas due to the Hyogoken-Nanbu earthquake, *Proceedings of the 19th Asian Conference of Remote Sensing*, C7, Asian Association on Remote Sensing, pp. 1–6.

Building Research Institute (BRI), 1996. *Final Report of Damage Survey of the 1995 Hyogoken-Nanbu Earthquake*, Building Research Institute (in Japanese).

Eguchi, R. T., Huyck, C. K., Houshmand, B., Tralli, D. M., and Shinozuka, M., 2000. A new application for remotely sensed data: Construction of building inventories using synthetic aperture radar technology, *Proceedings of the 2nd Multilateral Workshop on Development of Earthquake and Tsunami Disaster Mitigation Technologies and Their Integration for the Asia-Pacific Region*, Earthquake Disaster Mitigation Research Center, pp. 217–228.

Estrada, M., Matsuoka, M., and Yamazaki, F., 2000. Use of Landsat images for the identification of damage due to the 1999 Kocaeli, Turkey earthquake, *Proceedings of the 21st Asian Conference on Remote Sensing*, **2**, Asian Association on Remote Sensing, pp. 1185–1190.

Frost, V. S., Stiles, J. A., Shanmugan, K. S., and Holtzman, J. C., 1982. A model for radar im-

ages and its application to adaptive digital filtering of multiplicative noise, *Transactions on Pattern Analysis and Machine Intelligence*, PAMI-4 (24), Institute of Electrical and Electronics Engineers, 157–166.

Henderson, F. M., and Lewis, A. J., 1998. *Principles and Applications of Imaging Radar, Manual of Remote Sensing*, **2**, John Wiley & Sons, Inc., New York.

Ito, Y., Hosokawa, M., Lee, H., and Liu, J. G., 2000. Extraction of damaged regions using SAR data and neural networks, *Proceedings of 19th Congress of International Society for Photogrammetry and Remote Sensing (ISPRS2000)*, International Society for Photogrammetry and Remote Sensing, **33**, Part B1, pp. 156–163.

Lee, J. S., 1980. Digital image enhancement and noise filtering by use of local statistics, *Transactions on Pattern Analysis and Machine Intelligence*, PAMI-2 (2), Institute of Electrical and Electronics Engineers, 165–168.

Maki, N., Horie, K., Hayashi, H., and Tanaka, S., 2001. Physical damage level comparison of the damage assessment results in the Hanshin-Awaji Earthquake Disaster, *Journal of Social Safety Science, Institute of Social Safety Science,* **3**, 117–122 (in Japanese).

Massonnet, D., Feigl, K. L., Vadon, H., and Rossi, M., 1996. Coseismic deformation field of the M=6.7 Northridge, California, earthquake of January 17, 1994, recorded by two radar satellites using Interferometry, *Geophys. Res. Lett.* **23** (9), 969–972.

Massonnet, D., Rossi, M., Carmona, C., Adragna, F., Peltzer, G., Fiegl, K., and Rabaute, T., 1993. The displacement field of the Landers earthquake mapped by radar interferometry, *Nature (London)* **364**, 138–142.

Matsuoka, M., and Yamazaki, F., 1998. Identification of damaged areas due to the 1995 Hyogoken-Nanbu earthquake using satellite optical images, *Proceedings of the 19th Asian Conference of Remote Sensing*, Q9, Asian Association on Remote Sensing, pp. 1–6.

Matsuoka, M., and Yamazaki, F., 2000a. Use of interferometric satellite SAR for earthquake damage detection, *Proceedings of the 6th International Conference on Seismic Zonation*, Earthquake Engineering Research Institute, pp. 103–108.

Matsuoka, M., and Yamazaki, F., 2000b. Interferometric characterization of areas damaged by the 1995 Kobe earthquake using satellite SAR images, *Proceedings of the 12th World Conference on Earthquake Engineering*, **2**, CD-ROM, ID2141.

Murakami, M., Tobita, M., Fujiwara, S., Saito, T., and Masaharu, H., 1996. Coseismic crustal deformations of 1994 Northridge, California earthquake detected by interferometric JERS-1 synthetic aperture radar, *J. Geophys. Res.,* **101**, 8605–8614.

Ozawa, S., Murakami, M., Fujiwara, S., and Tobita, M., 1997. Synthetic aperture radar interferogram of the 1995 Kobe earthquake and its geodetic inversion, *Geophys. Res. Lett.* **24** (18), 2327–2330.

Rosen, P. A., Hensley, S., Peltzer, G., Rignot, E., and Werner, C., 1999. JERS-1 synthetic aperture radar interferometry applications—Mapping of rain forest environment and crustal deformation studies, *JERS-1 Science Program '99 PI Reports, Global Forest Monitoring and SAR Interferometry*, National Space Development Agency of Japan, 179–184.

Shinozuka, M., and Rejaie, A., 2000. Correlational analysis of remotely sensed pre- and post-disaster images, *SPIE's 7th Annual International Symposium on Smart Structures and Materials*, Society of Photo-Optical Instrumentation Engineers.

Shinozuka, M., Ghanem, R., Houshmand, B., and Mansouri, B., 2000. Damage detection in urban areas by SAR imagery, *J. Eng. Mech.* **126** (7), 769–777.

Sudo, N., Tada, T., Nakano, R., Cho, K., Shimoda, H., and Sakata, T., 1995. Multi-stage remote

sensing on the Great Hanshin earthquake disaster survey, *Proceedings of the 18th Japanese Conference on Remote Sensing*, Remote Sensing Society of Japan, pp. 115–116 (in Japanese).

Tralli, D., 2000. Assessment of advanced technologies for loss estimation, *Technical Report MCEER-00-SP02*, Multidisciplinary Center for Earthquake Engineering Research, State University of New York, Buffalo, NY.

Ulaby, F. T., Moore, R. K., and Fung, A. K., 1982. *Microwave Remote Sensing: Active and Passive, Volume II Radar Remote Sensing and Surface Scattering and Emission Theory*, Artech House.

Yamazaki, F., and Matsuoka, M., 1999. Remote sensing: Assessing the built environment by remote sensing technologies, *Proceedings of the 2nd International Workshop on Earthquakes and Megacities*, Earthquakes and Megacities Initiative (EMI), pp. 27–34.

Yonezawa, C., and Takeuchi, S., 1999. Detection of urban damage using interferometric SAR decorrelation, *Proceedings of International Geoscience and Remote Sensing Symposium*, **2**, Institute of Electrical and Electronics Engineers, pp. 925–927.

Yonezawa, C., and Takeuchi, S., 2001. Decorrelation of SAR data by urban damages caused by the 1995 Hyogoken-Nanbu earthquake, *International Journal of Remote Sensing* **22** (8), 1585–1600.

Zebker, H. A., and Villasenor, J., 1992. Decorrelation in interferometric radar echoes, *Transactions on Geoscience and Remote Sensing, Institute of Electrical and Electronics Engineers,* **30** (5), 950–959.

(Received 28 January 2002; accepted 2 February 2004)